Hindawi Publishing Corporation
International Journal of Photoenergy
Volume 2015, Article ID 919217, 13 pages
http://dx.doi.org/10.1155/2015/919217

Research Article

Efficacy of the Reactive Oxygen Species Generated by Immobilized TiO_2 in the Photocatalytic Degradation of Diclofenac

B. Di Credico,[1] I. R. Bellobono,[2] M. D'Arienzo,[1] D. Fumagalli,[1] M. Redaelli,[1] R. Scotti,[1] and F. Morazzoni[1]

[1]*Department of Material Science, INSTM, HINT-COST Project, University of Milano-Bicocca, Via R. Cozzi 55, 20125 Milano, Italy*
[2]*LASA, Department of Physics, University of Milan, Via Fratelli Cervi, 20090 Segrate, Italy*

Correspondence should be addressed to B. Di Credico; barbara.dicredico@unimib.it

Received 14 March 2015; Revised 8 May 2015; Accepted 12 May 2015

Academic Editor: Dionissios Mantzavinos

We report on the photodegradation of diclofenac (DCF) by hydrothermal anatase nanocrystals either free or immobilized in porous silica matrix (TS) in connection to the type and amount of reactive oxygen species (ROS), in order to have deeper insight into their role in the photocatalysis and to provide an effective tool to implement the DCF mineralization. TiO_2 and TS exhibit a remarkable efficiency in the DCF abatement, supporting that the utilization of anatase nanoparticles with the highly reactive {001}, {010}, and {101} exposed surfaces can be an effective way for enhancing the photooxidation even of the persistent pollutants. Furthermore, the hydrothermal TiO_2, when immobilized in silica matrix, preserves its functional properties, combining high photoactivity with an easy technical use and recovery of the catalyst. The catalysts performances have been related to the presence of $OH^{\bullet}$, $^1O_2$, and $O_2^{-\bullet}$ species by electron paramagnetic resonance spin-trap technique. The results demonstrated that the ROS concentration increases with the increase of photoactivity and indicated a significant involvement of $^1O_2$ in the DCF degradation. The efficacy of TiO_2 when immobilized on a silica matrix was associated with the high ROS life time and with the presence of singlet oxygen, which contributes to the complete photomineralization of DCF.

1. Introduction

The access to safe drinking water is essential for human well-being and sustainable development. In the last decade, the spread of micropollutant contamination in many freshwater reservoirs is becoming a serious threat for the environment and human health [1, 2]. In fact, pharmaceuticals, for example, analgesics, anti-inflammatories, beta-blockers, antidiabetics, and X-ray contrast media, are partially metabolized by the human body and remain in water resources [3]. Diclofenac (DCF), ciprofloxacin, erythromycin, ibuprofen, and naproxen are the most commonly detected drugs, due to their large use and introduction into the aquatic environment through human and animal excretions, but also resulting from the unused medications if improperly disposed [4]. Since these pharmaceuticals have long half-lives in the environment, they frequently accumulate, reaching biologically active levels [5].

DCF (2-[2,6-(dichlorophenyl)amino]phenyl acetic acid), a nonsteroidal anti-inflammatory drug [6], has a global consumption of 940 tons per year in the form of capsules, suppositories, tablets, and intravenous solution [7]. Since this drug is not completely metabolized after consumption and it is only partially degraded in treatment plants exploiting conventional and advanced cleaning technologies [8], high concentrations (up to 21.6 μg/L) of DCF have been detected in municipal wastewater effluent, surface water, groundwater, and drinking water [7].

Among the advanced cleaning processes [9–11], TiO_2-promoted photocatalysis seems a very promising approach

toward the effective degradation of several pharmaceutical micropollutants [11–14]. Recently, the DCF photocatalytic treatment by different TiO_2-based catalysts has been reported [15, 16]. In all the examined cases, only 85% of DCF conversion was attained; in fact, the DCF degradation pathway is very complex and includes the formation of partially oxidized products with higher toxicity than the parent compound [17].

It is well known that the TiO_2 photocatalytic mechanism involves the so-called *reactive oxygen species* (ROS), that is, hydroxyl radicals ($OH^\bullet$), hydroperoxyl radical ($HO_2^\bullet$), hydrogen peroxide (H_2O_2), singlet oxygen ($^1O_2$), and superoxide ($O_2^{-\bullet}$) [18–24]. Upon UV-Vis irradiation, TiO_2 converts the incoming photons into electron/hole pairs, which can either recombine or migrate to the material surface, where they can generate ROS and activate redox reactions. $OH^\bullet$ radicals are the most powerful oxidizing species, and they are considered the first responsible for the photodegradation processes in aqueous solution. $O_2^{-\bullet}$ has less oxidizing properties but generates $^1O_2$, which acts as powerful selective oxidant in the photosensitized transformation of organic substances [25–27]. In particular, organic pollutants including polycyclic aromatic hydrocarbons or chlorophenols, such as DCF, are considerably vulnerable to singlet oxygen since the electrophilic $^1O_2$ species easily oxidizes the electron-rich olefins, dienes, neutral nucleophiles such as amines, and aromatic hydrocarbons anions [28–30]. Nowadays, TiO_2-based photocatalytic treatments of DCF are far from being optimized and a better knowledge of type and amount of ROS implied in the degradation mechanism may provide an effective tool to optimize mineralization.

Moreover, the photodegradation reactions are usually performed by using TiO_2 nanoparticles in aqueous suspension (slurry), which causes difficult postuse recovery of the catalyst and requires expensive and time-consuming separation/recycling processes [18, 31]. TiO_2 nanoparticles when dispersed in the surrounding environment may be also hazardous, due to their potential inflammatory and cytotoxic effects [32].

In view of the above considerations, the present study reports on the DCF photocatalytic abatement in water, by using anatase nanoparticles with highly reactive crystal surfaces [33–35], either free [36] or suitably immobilized in a highly porous silica matrix [37].

Anchoring these nanocrystals onto the highly porous silica channels of the TiO_2-SiO_2 composite (TS) provides easy accessibility of surface sites as well as easy adsorption/interaction of the drug. Minimum deactivation, thermal stability, no TiO_2 leaching, and an easy scale-up of the process for domestic/civil water treatments are also important advantages associated with the employment of this immobilized catalyst.

The degradation of DCF and its transformation products was followed by UV-Vis spectroscopy, being able to identify the most persistent transformation products. The complete photomineralization was assessed by measuring the total organic carbon (TOC) at different reaction times. The ROS species, $OH^\bullet$ and $^1O_2$, formed by UV irradiation of the catalysts, were detected by Electron Paramagnetic Resonance (EPR) spin-trap technique. The ROS formation rate and their amount were related to the photoefficiency of both catalysts. Singular and unexpected stability properties have been found for the oxygenated radicals in TS, elucidating a role of the immobilization procedure in preserving the functional properties of the photoactive oxide.

2. Materials and Methods

2.1. Chemicals. DCF sodium salt and all chemicals were purchased from Sigma-Aldrich and used as received without further purification. Milli-Q water (MQ, resistivity 18.2 MΩ·cm at 25°C and TOC ≤ 5 μg/L) was used for the procedures that require water.

2.2. Synthesis and Functionalization of TiO_2 Nanoparticles. Anatase nanocrystals were obtained according to a previously reported procedure [36]. The TiO_2 surface was then functionalized with 2-methoxyethylamine by refluxing the suspension of the oxide with the organic reagent [37].

2.3. Preparation of TiO_2-SiO_2 Composite. As reported in our previous study [37], TS was prepared by inducing the sol-gel transition of the SiO_2 precursor, tetramethylortosylicate (TMOS), in the presence of the functionalized TiO_2 nanoparticles and polyethylene glycol, PEG (see Figure S1 in Supplementary Material available online at http://dx.doi.org/10.1155/2015/919217).

In the present study, TS composite was produced with a pellet shape, in order to be handily used in reactor and plants. Pellets were obtained by casting the precursor sol-phase in a suitable Teflon mold, constituted by several separated cylindrical holes (average diameter and average depth 0.5 cm). After ageing, the gel phase filling the holes was dried at 150°C for 1 h and finally calcined in air at 500°C for 5 h. This allows us to obtain TS pellets where TiO_2 nanocrystals lie at the surface of macroporous cavities inside the SiO_2 matrix.

2.4. Morphological and Chemical Characterization of TiO_2 Nanoparticles and TS Composite. The structure and the morphological features of both TiO_2 nanoparticles and TS composite were checked by using X-Ray Diffraction (XRD), Scanning Electron Microscopy (SEM), and Transmission and High-Resolution Transmission Electron Microscopy (TEM/HRTEM). The experimental conditions and the analytical details are previously reported [36, 37]. Specific surface area (SSA) and pore size distribution of micro- and mesopores were also checked in both TiO_2 and TS samples and compared to the previously reported results [36, 37].

2.5. Photoinduced Degradation of DCF. Photodegradation experiments employing TiO_2 nanoparticle slurry as catalyst were carried out in a 600 mL Pyrex discontinuous batch reactor with an external cooling jacket enveloped by an aluminum foil, equipped with a UV-Vis lamp placed in a coaxial quartz cylinder. The 125 W Hg high pressure lamp was used for UV-visible excitation (emission lines at λ = 254, 313,

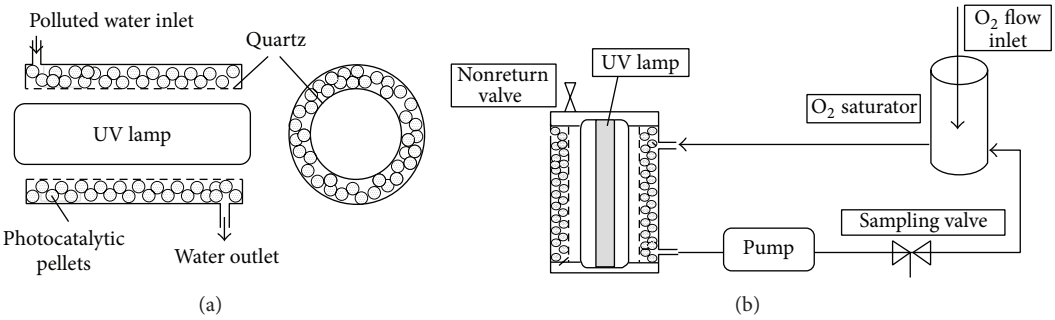

Figure 1: (a) Scheme of the photoreactor and the arrangement of the porous TS pellets (lateral and vertical cross-section views). (b) Schematic view of the photocatalytic plant.

366 (main), 405, and 436 nm). No optical filter was adopted. The photocatalytic experiments were carried out by using the DCF concentrations 2.0, 20.0, and 50 mg/L to confirm the reaction mechanism, the kinetics of the process, and the reaction products. Titania nanocrystals (160 ± 5 mg, $0.25\,g\,L^{-1}$) were suspended by ultrasound in 600 mL of water containing DCF at the concentrations reported above and recirculated by a peristaltic pump ($14\,mL\,s^{-1}$). The temperature was kept at $25 \pm 2^{\circ}C$.

When employing TS, the pellets were arranged inside the cylindrical photoreactor, shown in Figure 1, to facilitate both direct and diffuse light irradiation. For the photocatalytic experiments, 600 mL of water containing DCF at the concentrations reported above was recirculated in the presence of approximately 1.20 ± 0.05 g of TS (TiO_2 loading 0.128 g, corresponding to $0.21\,g\,L^{-1}$) as described in Figure 1(b) [38].

The photocatalytic experiments were carried out also employing TS powder in slurry. In all cases, the aqueous phase was saturated by continuously bubbling oxygen (constant feed = $100\,mL\,min^{-1}$) in an online chamber and circulated in the dark for 30 min before turning on the UV-Vis source. The excess of gas was eliminated through nonreturn check valve. Control experiments were carried out in the absence of TiO_2 (Blank). The photocatalytic degradation was followed firstly by UV-Vis spectroscopy. Aliquots (6 mL) of the reaction solution were drawn out at regular intervals, and the centrifuged clear solutions were utilized to record the spectra under the following conditions: wavelength range: 190–400 nm, scan rate: $600\,nm\,min^{-1}$, time response: 0.1 s, and spectral band: 2 nm (Varian Cary 4000 Spectrophotometer). The DCF complete mineralization was analyzed by measuring TOC with a Shimadzu TOC-V CSH analyzer.

2.6. Spin-Trap EPR Experiments. Spin-trap experiments were performed to detect the short-living ROS, namely, $O_2^{-\bullet}$, $OH^{\bullet}$, and $^1O_2$, in the reaction aqueous medium. The reagent to reveal the $^1O_2$ species was 2,2,6,6-tetramethyl-4-piperidine (TEMP), whereas 5,5-dimethyl-1-pyrroline-N-oxide (DMPO) simultaneously detects $O_2^{-\bullet}$, $OH^{\bullet}$, and $^1O_2$. In order to distinguish the contribution of $^1O_2$ and $O_2^{-\bullet}$, from that of $OH^{\bullet}$, a typical $OH^{\bullet}$ radical scavenger, DMSO (50 mM), was employed. Spectra were acquired before and during the UV-Vis irradiation in the EPR cell.

The stock suspensions were prepared by dispersing TiO_2 and TS in powder form in MQ water (20 mM in TiO_2) and carefully homogenizing them in ultrasound bath (1 h). Then, the appropriate spin-trap agent (concentration: 20 mM) was added.

The stock solution in a reservoir was purged for 30 min with pure O_2 before the experiment and then, just a few minutes before irradiation, was pumped into the EPR cell (6 cm window length, 0.5 mm optical path) through a Teflon tube directly connected to the reservoir. EPR investigation was performed at 293 K by a Bruker EMX spectrometer working at the X-band frequency. The irradiation source was a UV-Vis 150 W Xe lamp with the output radiation focused on the samples in the cavity by an optical fiber (50 cm length, 0.3 cm diameter). The g values were calculated by standardization with α,α'-diphenyl-β-picrylhydrazyl (DPPH).

Typical EPR spectrometer settings were microwave frequency 9.8 GHz; microwave power 10 mW; sweep width 6–10 mT; modulation amplitude 0.05–0.2 mT; scan time 20.97 or 41.94 s; time constant 40.96 or 81.92 ms.

The maximum intensity of the first derivative peak of the spin-trapped signal was plotted against the reaction time in order to follow the ROS production in the irradiated suspensions. The initial slope (r_o), calculated as tangent of the curve at the beginning of the adduct formation, was taken as representative parameter [26] of the ROS formation rate.

3. Results and Discussion

3.1. Structural and Morphological Characterization of TiO_2 and TS Catalysts. XRD patterns of both TiO_2 and TS catalysts indicate the exclusive presence of the anatase phase (Figure S2).

In order to check the correspondence with the solids reported in our previous paper [36], TEM and HRTEM images of TiO_2 nanocrystals were collected (Figure 2(a)). No internal pores or amorphous surface layers were detectable. Particles show almost square or rectangular shapes with aspect ratio α (α = length/width) of about 1–3.

Higher magnification (inset in Figure 2(a)) of the lattice fringes along the [010] direction clearly reveals the presence of (002) crystallographic planes with lattice space of 0.48 nm. This indicates that TiO_2 nanocrystals mainly expose the high-energy {001} and {010} facets, even if smaller amounts of

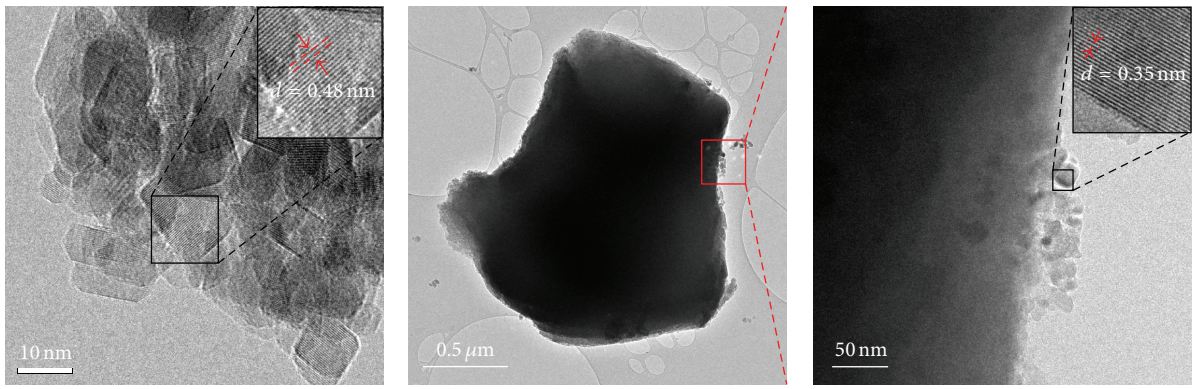

(a) (b) (c)

FIGURE 2: TEM and HRTEM images of TiO_2 (a) and TS composite (b, c). Details on crystallographic planes detected are shown in the inset of (a) and (c).

thermodynamically stable and lower energy {101} surfaces are detectable (see further TEM and HRTEM images in Figure S3). According to the literature [39–42], anatase {001}, {010}, and {101} faces are thought to be differently involved in the photooxidation, due to their different surface energy, and are responsible for the high reactivity of hydrothermal TiO_2 [18, 34, 41]. In particular, the {001} surfaces display the highest density of undercoordinated Ti centers and enlarged O-Ti-O bond angles, which increases the surface energy and makes titanium and oxygen centers very reactive in photooxidation reactions [39, 41]. In addition, we have recently proved that also the {101} surfaces contribute to the oxidation processes *via* the formation of the superoxide species [41]. Besides, Pan et al. [34] reported that particles, where the {001} surfaces are copresent with a high percentage of {010} facets, promote the generation of OH radicals.

The morphology of TS was also investigated and compared with the results of our previous study. SEM micrographs (Figure S4) show that the average diameter of silica particles in the matrix is about 2.5 μm and confirm the presence of an interconnected macroporous structure. TEM and HRTEM images of TS (Figures 2(b) and 2(c)) show that TiO_2 nanocrystals are anchored to the surface of silica channels without forming large aggregates and maintain their pristine size, shape, and exposed {001}, {010}, and {101} crystals facets (inset in Figure 2(c)).

Nitrogen physisorption experiments performed on TS samples revealed the occurrence of a type IV isotherm with a wide hysteresis loop, suggesting a remarkable mesopores contribution (Figure S5) to the total surface area. The pore size distribution (inset in Figure S5) supports the existence of mesopores, due to the TiO_2 nanocrystals [37], with an average pore diameter centred at 3.6 nm.

3.2. Photodegradation of DCF: UV-Vis Spectroscopy Investigation. The photodegradation of DCF in the presence of TiO_2 or TS was firstly followed by UV-Vis absorption spectroscopy (Figures 3(a) and 3(b)), compared to that in the absence of catalyst (see Figure S6). Several DCF transformation products were identified.

In the case of pure TiO_2, the absorption spectrum of DCF initially (time = 0 min) shows a single band centred at 279 nm (solid line in Figure 3(a)). This feature disappears after 2 min of UV-Vis irradiation (dashed lines in Figure 3(a)) and simultaneously four new bands at 210, 240, 289, and 324 nm become detectable (dashed lines in Figure 3(a)). According to the literature [43], these features can be unambiguously assigned to the monohalogenated carbazole (DCF-DP1, Figure 3(c)), resulting from the loss of one chlorine atom followed by intramolecular cyclization of DCF.

After 10 min of irradiation, the DCF-DP1 absorption peaks gradually decrease in intensity (dotted lines in Figure 3(a)) and slightly shift toward higher wavelengths. This may suggest that the chromophoric carbazole structure remains basically unaffected along the reaction time, and the photodegradation probably progresses through the formation of the DCF-DP2 and DCF-DP3 intermediates (Figure 3(c)), as already observed in the literature under similar reaction conditions [3, 43]. DCF-DP2 and DCF-DP3 products have in fact a carbazole-based structure whose π-conjugated condensed rings possess high stability and therefore are recalcitrant to further degradation. The formation of carbazoles, recently assessed for DCF photobiodegradation in an aquatic environment under solar light irradiation, is particularly undesired due to their remarkable phytotoxicity [44]. After 120 min reaction time, the spectral features attributed to carbazole species became very weak and poorly resolved (dotted-dashed line in Figure 3(a)).

In the presence of TS catalyst, a similar spectral behavior has been observed (Figure 3(b)). In this case, the starting drug was transformed in DCF-DP1 after a higher irradiation time (10 min) than that for pure anatase (dotted lines in Figure 3(b)). However, the spectrum shows that the immobilized system was able to remove DCF and its recalcitrant photoproducts after 120 min (dotted-dashed line in Figure 3(b)), as well as the pure TiO_2 in slurry.

On the contrary, in the Blank experiment (Figure S6), the UV-Vis spectra show intense and very stable peaks relatable to DCF-DP1 and DCF-DP2 till the end of the reaction time.

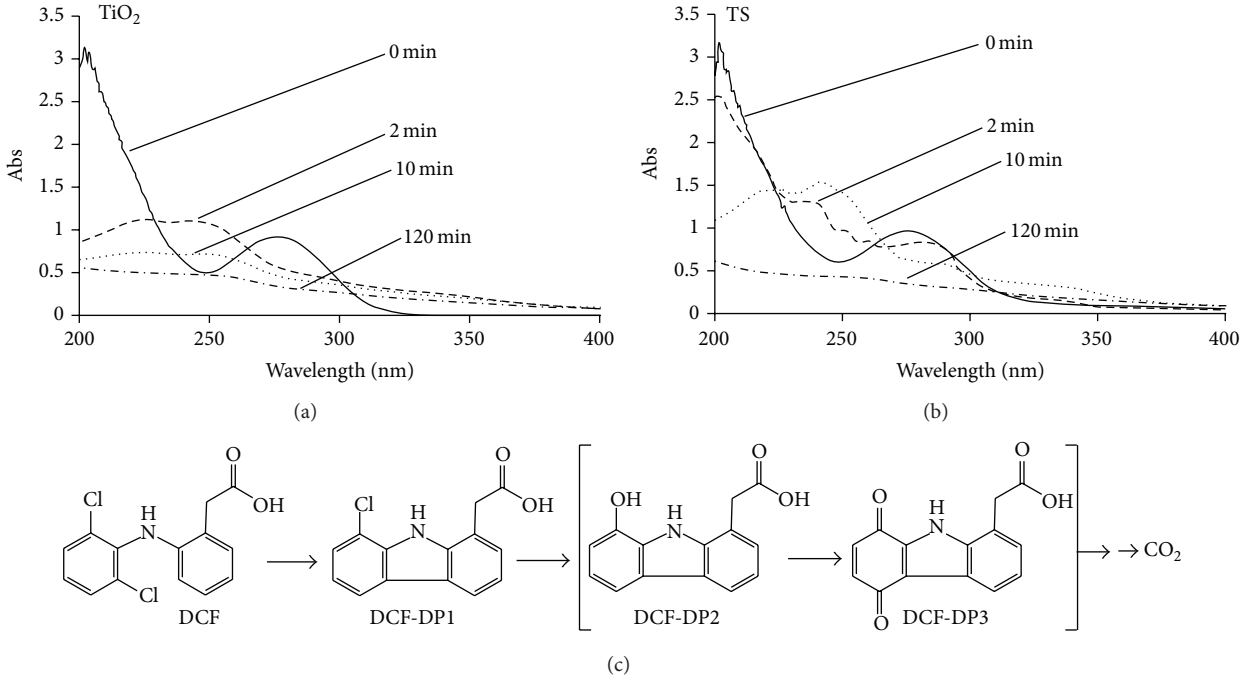

Figure 3: Selected absorption spectra of DCF recorded at different reaction times in the presence of (a) TiO_2 and (b) TS. (DCF (solid line), with photoreaction spectra after 2 min (dashed line), 10 min (dotted line), and 120 min (dotted-dashed line)). (c) Photodegradation pathway proposed for DCF in the presence of TiO_2 and TS catalysts with hypothesized carbazole *intermediates*, shown in *square brackets*.

This suggests that the utilized catalysts favour the breakdown of the carbazole structures and the complete drug degradation.

3.3. Photomineralization of DCF: TOC Analysis. In order to assess the complete mineralization of DCF, a TOC analysis was performed. During the initial stage of recirculation in the dark (30 min), the chemisorption of the drug on the catalyst surface caused a TOC depletion of about 4.0 ± 2%. The experimental data obtained by using either TiO_2 or TS are shown in Figure 4. The Blank test is also reported for comparison.

For TiO_2 nanocrystals, a sharp decrease of the TOC percentage is observed in the first 10 min of the reaction. After 30 min, the degradation apparently brakes and then, only at higher reaction times ($t > 120$ min), a sharp TOC decay again occurs. In the case of TS composite, the DCF photodegradation is initially slow, while after a reaction time of 50 min a significant decay of the TOC amount is noticeable (Figure 4).

These results are consistent with the degradation mechanism proposed for DCF on the basis of UV-Vis analysis. In the presence of TiO_2 nanocrystals, the sharp decrease of the TOC percentage in the first minutes of the process corresponds to the formation of subproducts, probably deriving from DCF decarboxylation and/or dealkylation reactions. Afterwards, the decrease of the degradation rate, observed at different reaction times for TiO_2 and TS samples, may be attributed to the persistent presence of hypothesized halogenated carbazole (DCF-DP1) and of DCF-DP2 and

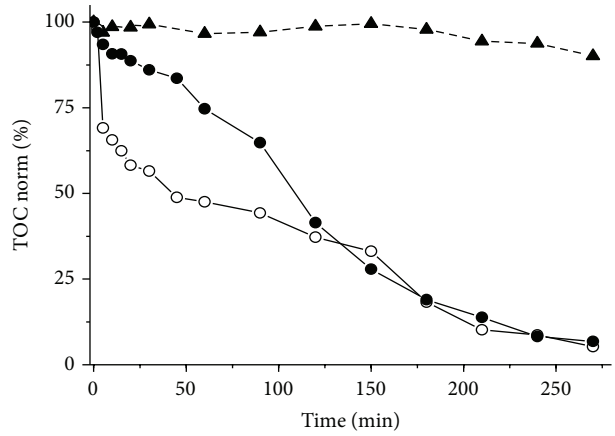

Figure 4: Mineralization curves (given as TOC%) of DCF (50 mg/mL) under UV-Vis irradiation in the presence of O_2 for (▲) Blank, (○) TiO_2, and (●) TS in slurry.

DCF-DP3 carbazole molecules and to their recalcitrant phototransformation products, which presumably originate from the loss of the carboxylic group and the alkyl chain, followed by the breaking of aromatic rings and formation of alkane derivatives. This behavior is more remarkable and evident for TS, rather than TiO_2 alone. However, at the end of the process, DCF is completely mineralized by both employing TS and TiO_2 catalysts, whereas the degradation is negligible under simple photolytic condition (Figure 4).

It is interesting to note that the complete mineralization of the drug occurs in very similar times for both TiO_2 and

TS catalysts. This is again in agreement with the UV-Vis results and demonstrates the efficacy of the immobilization procedure in preserving the peculiar photoactivity of TiO_2. The same behavior has already been observed in the photomineralization of the phenol [18, 37] and was ascribed to the high dispersion of catalyst nanocrystals at the surface of silica macropores, which guarantees high accessibility of the catalyst at the solid-liquid interface and intimate contact between the substrate molecules and the nanoparticles.

In order to compare the mineralization kinetics of DCF using TiO_2 or TS catalysts, the half degradation time ($t_{1/2}$), that is, the reaction time at which the TOC reaches 50%, was used as the representative parameter. Even if the best catalytic performance occurs for pure TiO_2 ($t_{1/2} = 50$ min), the TS composite displays an efficiency ($t_{1/2} = 110$ min) much higher than the Blank (estimated $t_{1/2} > 500$ min). These results suggest that the utilization of anatase nanocrystals with {001}, {010}, and {101} exposed surfaces, either free or immobilized in silica matrix, can enhance the photooxidation reactions, even for those of the very stable substrates like DCF or carbazoles. The negligible DCF degradation is in the absence of catalyst and is in agreement with the reported high stability of DCF, for which complete photomineralization is difficult to achieve by conventional water treatments [15–17].

The satisfactory performances of immobilized catalyst confirm that the immobilization procedure preserves the catalytic properties of TiO_2 even for the abatement of the highly stable pharmaceuticals and simultaneously guarantees the benefits related to the use of a supported catalyst.

3.4. Kinetics of DCF Photodegradation for TS Composite and TiO_2 Nanocrystals. In order to obtain deeper insight into the photodegradation mechanism, the four-parameter kinetic model, proposed by Rota et al. for the partly heterogeneous oxidation of different complex organic substrates [45], was here applied to the DCF photomineralization (50 mg/L) catalyzed by either TiO_2 nanocrystals or TS composite.

According to this model, the DCF mineralization to CO_2 was assumed to occur through a single intermediate I, which contains the contribution of all intermediates:

$$\mathrm{DCF} \longrightarrow \mathrm{I} \longrightarrow \mathrm{CO_2}. \tag{1}$$

A system of first-order differential equations describes the variation of DCF, I, and CO_2 concentrations [46, 47]:

$$\left(\frac{dC}{dt}\right) = \frac{-k_1 \cdot K_1 \cdot C}{1 + K_1 \cdot C + K_2 \cdot C_\mathrm{I}},$$
$$\left(\frac{dC_\mathrm{I}}{dt}\right) = \frac{k_1 \cdot K_1 \cdot C \cdot k_2 \cdot K_2 \cdot C_\mathrm{I}}{1 + K_1 \cdot C + K_2 \cdot C_\mathrm{I}}, \tag{2}$$
$$\left(\frac{dC_{\mathrm{CO_2}}}{dt}\right) = \frac{k_1 \cdot K_1 \cdot C_\mathrm{I}}{1 + K_1 \cdot C + K_2 \cdot C_\mathrm{I}},$$

where C, C_I, and $C_{\mathrm{CO_2}}$ are the concentrations of DCF, I, and CO_2; K_1 and K_2 are the apparent chemisorption constants related to the competitive absorption of DCF and I, respectively, onto TiO_2 surface, and k_1 and k_2 represent the kinetic constants of the DCF and I degradation.

According to Figure 4, when the photodegradation in the presence of TS composite starts, C_I is negligible with respect to C, and the kinetic equations can be approximated to

$$\left(\frac{dC}{dt}\right) = -\frac{k_1 \cdot K_1 \cdot C}{1 + K_1 \cdot C}. \tag{3}$$

At the beginning of the process, the term $K_1 C > 1$ ($C_{(0)} = 1.57 \cdot 10^{-4}$ M and the order of magnitude of K_1 for DCF may be assumed very high) and (4) can be further simplified to a pseudo zero-order kinetic equation:

$$\left(\frac{dC}{dt}\right) \approx -k_{(0)}, \tag{4}$$

where $k_{(0)} = k_1$ is the pseudo zero-order kinetic constant.

Integrating between reaction times $t = 0$ and t results in

$$C - C_{(0)} \approx -k_{(0)} t. \tag{5}$$

Considering that at the very early stages of reaction the total organic carbon concentration may be assumed $C_\mathrm{TOC} \approx 14$ C, as DCF contains 14 carbon atoms, and that the very small concentrations of intermediates have structures very similar to the parental drug, (5) can be written as follows:

$$C_\mathrm{TOC} - C_{\mathrm{TOC}(0)} \approx -k_{(0)} t \tag{6}$$

by expressing the DCF concentration in terms of carbon concentration.

Coherently, the plot of $(C_\mathrm{TOC} - C_{\mathrm{TOC}(0)})$ *versus* reaction time (t) for the photodegradation of DCF in the presence of TS composite proves that, for reaction times below 50 min, the reaction follows an apparent zero-order (Figure 5(a)).

On the other hand, at a time $t^* > 50$ min, when $C \ll C_\mathrm{I}$, the kinetic equation (6) can be simplified to the following:

$$\left(\frac{dC_\mathrm{I}}{dt}\right) = -\frac{k_2 \cdot K_2 \cdot C_\mathrm{I}}{1 + K_2 \cdot C_\mathrm{I}}. \tag{7}$$

When C_I is very small, (7) becomes a pseudo first-order kinetic equation, where $k_{(1)} = k_2 K_2$ is the pseudo first-order kinetic constant:

$$\left(\frac{dC_\mathrm{I}}{dt}\right) \approx -k_{(1)} C_\mathrm{I}. \tag{8}$$

By integrating between t^* and t we obtain

$$\ln \frac{C_\mathrm{I}}{C_{\mathrm{I}(t^*)}} \approx -k_{(1)} t. \tag{9}$$

By considering that when $C \ll C_\mathrm{I}$, $C_\mathrm{I} \approx C_\mathrm{TOC}$ and that $C_{\mathrm{I}(t^*)} \approx C_{\mathrm{TOC}(0)}$, (9) can be rewritten as

$$\ln \frac{C_\mathrm{TOC}}{C_{\mathrm{TOC}(0)}} \approx -k_{(1)} t. \tag{10}$$

Reporting the $\ln(C_\mathrm{TOC}/C_{\mathrm{TOC}(0)})$ versus reaction time (t), the first-order kinetics can be easily observed (Figure 5(b)). According to (6) and (10), $k_{(0)}$ and $k_{(1)}$ have been calculated

Table 1: Kinetic constants of TiO_2 nanocrystals and TS composite for the photomineralization of DCF.

Sample	$k_{(0)}$ (mol min^{-1})	$k_{(1)}$ (min^{-1})	$k_{in(1)}$ (min^{-1})	$k_{adv(1)}$ (min^{-1})	$k_{fin(1)}$ (min^{-1})
TiO_2	n.o.*	n.o.	1.3×10^{-2}	3.5×10^{-3}	1.4×10^{-2}
TS	5.0×10^{-6}	1.2×10^{-2}	n.o.	n.o.	n.o.

*Not observed.

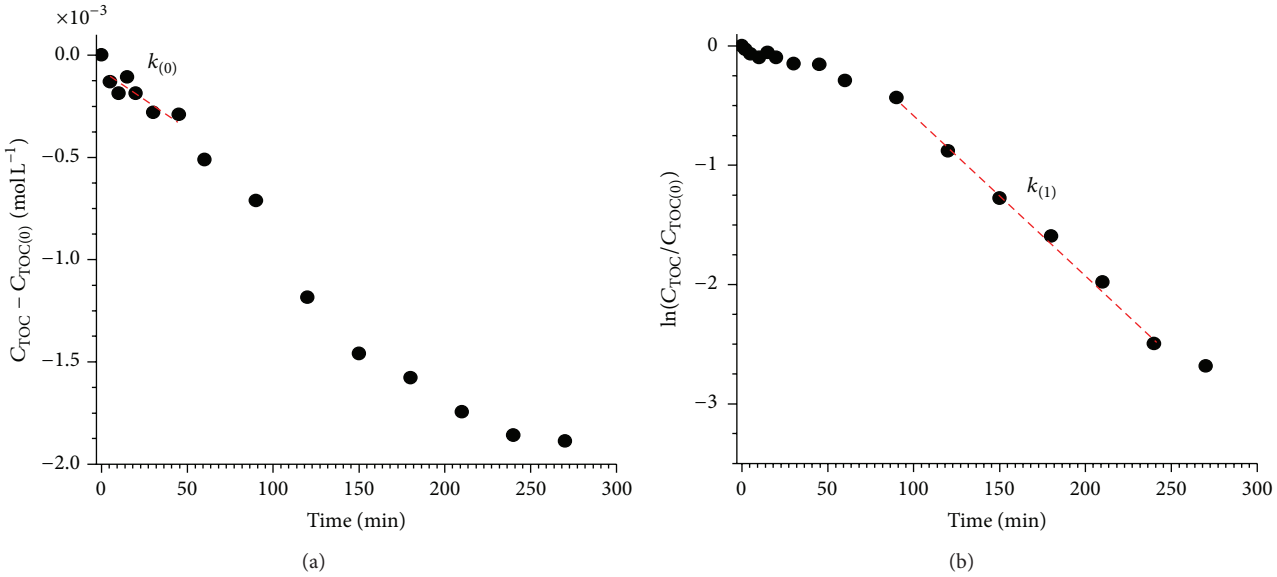

Figure 5: Plots of (a) ($C_{TOC} - C_{TOC(0)}$) and (b) ln($C_{TOC}/C_{TOC(0)}$) versus reaction time calculated from the experimental TOC versus time curves of DCF photomineralization in the presence of TS composite, according to (6) and (10).

from the slopes of the straight lines fitting the experimental points and reported in Table 1.

When the reaction is catalyzed by TiO_2 nanocrystals, the DCF degradation trend is different from that of TS (see Figure 4) and essentially follows an apparent first-order kinetics law. In fact, at the beginning of the process ($t <$ 50 min), C_I rapidly increases and therefore $C \ll C_I$. Consequently, a pseudo first-order kinetic law with a $k_{in(1)}$ ((8)-(9)) effectively describes the initial steps of the reaction. For $t^* \geq$ 50 min, the degradation slows down, but again an apparent first-order kinetics with a constant $k_{adv(1)}$, lower than $k_{in(1)}$, is the representative of the process. Finally, for a reaction time $t^* \geq 150$ min, the kinetic behavior for TiO_2 sample becomes very similar to that of TS; $k_{fin(1)}$ can be defined. Figure 6 shows the plot of the ln($C_{TOC}/C_{TOC(0)}$) versus reaction time (t) for the DCF degradation in the presence of TiO_2 nanocrystals. The values of the three different pseudo first-order kinetic constants have been calculated from the slopes of the straight lines fitting the experimental points and reported in Table 1.

Since the kinetic behaviors of the samples are very different for reaction times lower than 120 min, a fair comparison cannot be made by considering only the rate constants values, owing also to the above observations concerning the greater efficiency of TiO_2 with respect to TS and to the concentration effects, which may be different for intermediates of photodegradation in the different stages of the overall photocatalytic degradation process. However, it can be observed that the presence of first-order kinetics for TiO_2 nanocrystals is in agreement with its higher $t_{1/2}$ time in the DCF photomineralization.

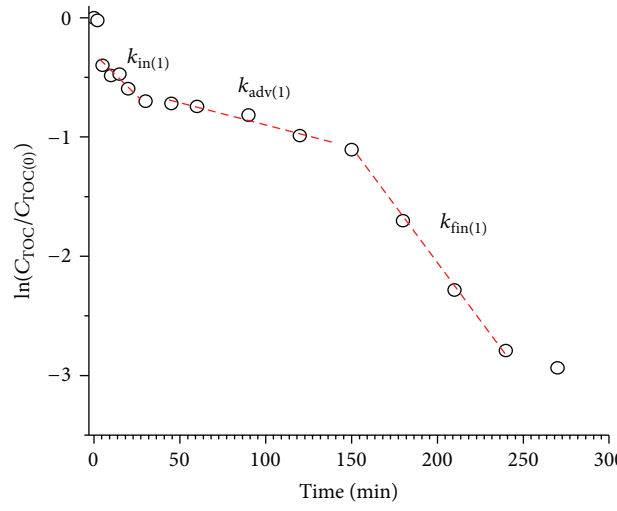

Figure 6: Plots of ln($C_{TOC}/C_{TOC(0)}$) versus reaction time calculated from the experimental TOC versus time curves of DCF photomineralization in the presence of TiO_2 nanocrystals, according to (6) and (10).

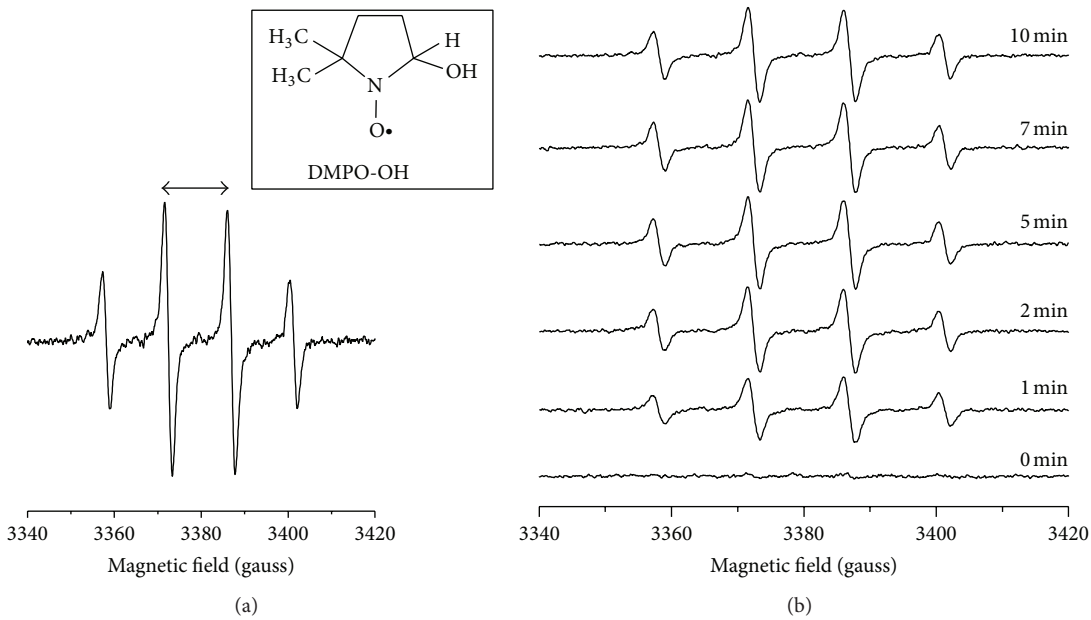

Figure 7: (a) EPR spectrum of the DMPO-OH adduct (structure shown in the inset). (b) Variation of the DMPO-OH resonance lines with the UV-Vis irradiation time for the TS aqueous suspension.

3.5. Study of ROS Species in the Presence of TiO_2 and TS Catalysts. The UV irradiation of TiO_2 in oxygenated aqueous media results in the generation of ROS ($OH^\bullet$, H_2O_2, $O_2^{-\bullet}$, and $^1O_2$), which are thought, at the molecular level, to be the active intermediates of the photooxidation processes [20–24]. Among them, $OH^\bullet$ has the highest oxidation potential ($E^\circ(OH^\bullet/H_2O) = +2.27$ V *versus* NHE at pH 7) [48], and it is believed to be the main responsible species for the photooxidation processes in aqueous solution. The photoproduced H_2O_2 also contributes to the formation of $OH^\bullet$ species, since it is rapidly photolyzed by UV irradiation. $^1O_2$ is instead a lower oxidant ($E^\circ(^1O_2/O_2^{-\bullet}) = +0.34$ V [49], while superoxide is essentially a poor oxidant $E^\circ(O_2/O_2^{-\bullet}) = -0.28$ V) [48]. Since both $^1O_2$ and $O_2^{-\bullet}$ demonstrate important selectivity in several reported photooxidative processes [26–30], it appears mandatory to investigate the nature and the amount of these species in our process.

A very suitable *in situ* method to determine these species exploits the spin-trapping agents, by using EPR for detection, due to the short ROS life times. The identification of hydroxyl radicals is usually performed by using DMPO as reactive probe [50–52]. The interaction of $OH^\bullet$ species with DMPO yields the $^\bullet$DMPO-OH adduct (inset in Figure 7(a)). $^\bullet$DMPO-OH displays a four-line EPR signal with Hamiltonian parameter $g = 2.0057$ and hyperfine splitting, $a_N = 1.495$ mT, $a_H^\beta = 1.472$ mT (Figure 7(a)), in agreement with a very large number of references [50, 51].

Recent studies [52, 53] have suggested that DMPO, in addition to reacting with $OH^\bullet$, can be oxidized by $^1O_2$ and $O_2^{-\bullet}$ to yield $^\bullet$DMPO-OH. Therefore, DMPO cannot selectively trap $OH^\bullet$, while it simultaneously reveals hydroxyl, superoxide, and singlet oxygen.

Aiming to find significant relationships between the presence of different ROS and the photoactivity of TiO_2-based catalysts in DCF photodegradation, the following experiments were performed.

Firstly, EPR spectra were recorded under UV-Vis irradiation in the presence of DMPO. In order to evaluate the contribution of superoxide and singlet oxygen to the $^\bullet$DMPO-OH signal, experiments were also performed in the presence of DMSO, a typical $OH^\bullet$ quencher [54].

At the beginning of irradiation, the $^\bullet$DMPO-OH adduct rapidly forms for both TiO_2 and TS catalysts, and the signal intensity increases over time (Figures 7(b) and 8(a)).

However, prolonged irradiation results in a decrease of the $^\bullet$DMPO-OH amount, probably due to the coupling of the radicals and/or to progressive oxidation of DMPO, as a result of the multiple addition of OH radicals producing EPR-silent products (Figure 8(a)) [51, 55, 56].

Thus, the maximum intensity of the EPR signal cannot be univocally associated with the amount of the ROS species and the initial slope r_o of the $^\bullet$DMPO-OH curve intensity *versus* time, corresponding to the initial rate of $OH^\bullet$, $O_2^{-\bullet}$, and $^1O_2$ formation (Figure 8(b)), was assumed as representative parameter.

Figure 8(b) shows that the TiO_2 has a higher r_o value than the TS sample, in agreement with the better performance observed for the titania nanocrystals in DCF photodegradation. However, comparing the curves in Figure 8(a), it must be highlighted that after 240 seconds the generation of $^\bullet$DMPO-OH species undergoes a fast decay in the presence of TiO_2 catalyst (black line), whereas for the TS catalyst it remains constant for at least 600 seconds since the beginning of the UV-Vis irradiation (red line).

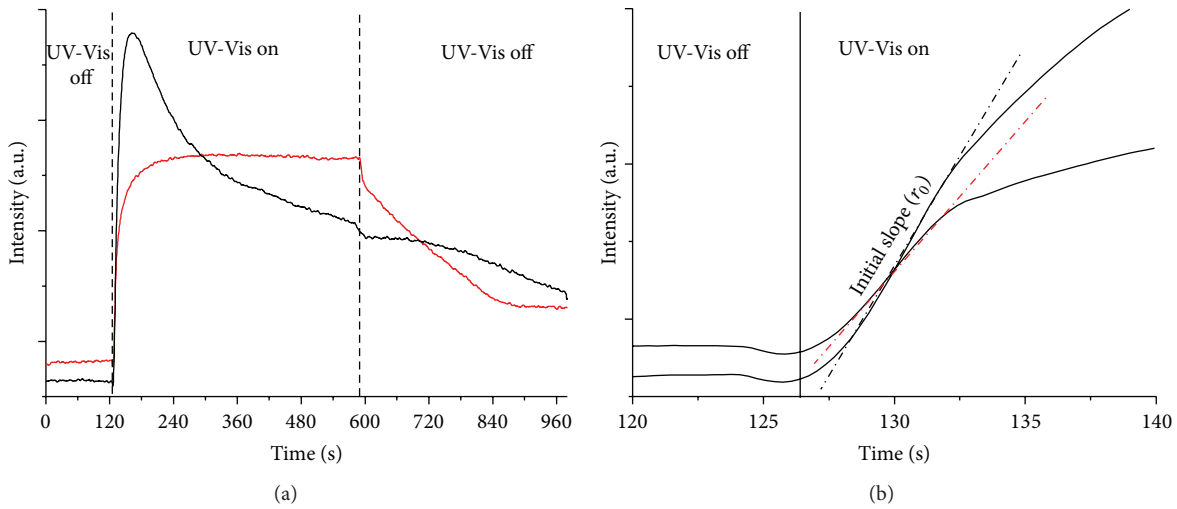

FIGURE 8: (a) Time course of the •DMPO-OH signal maximum before and during UV-Vis irradiation for TiO_2 (black line) and TS (red line) samples; (b) magnification of the initial portion of the curve for which the initial slope (r_o) was taken as representative parameter to evaluate the initial rate of OH•, $O_2^{-\bullet}$, and $^1O_2$ generation.

This suggests that the quenching of •DMPO-OH radicals is inhibited in the titania-silica composite. We may attribute such effect to the high macro-/mesoporosity of the silica channels which tune the DMPO/•DMPO-OH diffusion toward/from the catalytic active sites, thus making gradual their interaction with the highly dispersed TiO_2 nanocrystals. This may prevent either the coupling or the fast photooxidation of •DMPO-OH radicals. On the basis of the previous observations, we suggest that the anatase nanoparticles act as confined "nanoreactors," where the ROS species are formed and may easily interact with the DCF molecules before their annihilation.

After the addition of DMSO, a typical OH• radical quencher, to the aqueous suspensions of TiO_2 and TS, only a partial decrease of the •DMPO-OH signal was observed, while additional features attributable to DMPO-CH_3 (with hyperfine constant $a_N = 1.64$ mT, $a_H^{\beta} = 2.34$ mT, Figure 9) appear. This suggests that the generation of •DMPO-OH adduct upon UV-Vis irradiation of TiO_2 and TS derives from the trapping of ROS other than OH•. These radicals being stable in the presence of DMSO may be attributed mainly to the oxidation of DMPO operated by singlet oxygen (deriving from $O_2^{-\bullet}$), indicating a possible contribution of this species to the photodegradation mechanism.

While many papers support the relevance of $^1O_2$ in TiO_2-assisted photocatalytic processes [54–57], only few of them comprehensively describe the role of singlet oxygen species when the catalyst is immobilized [58].

Aiming to confirm the presence of this highly oxidant species in TiO_2 and TS suspensions, a second set of EPR experiments was carried out by using the TEMP spin trap, being able to evidence the $^1O_2$ species, giving the TEMPO radical (inset in Figure 10(a)) [59].

The obtained 2,2,6,6-tetramethyl-4-piperidone-N-oxyl (TEMPO) species is characterized by a typical three-line EPR signal with hyperfine constant $a_N = 1.63$ mT and $g = 2.006$.

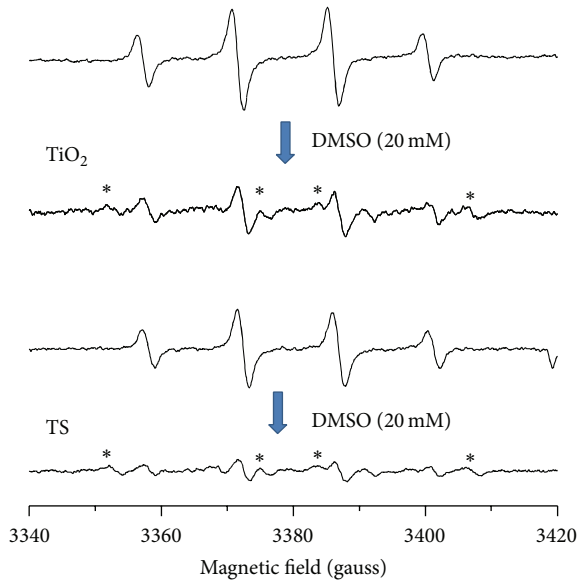

FIGURE 9: Effect of DMSO on the •DMPO-OH signal during UV-Vis irradiation of aqueous suspensions of TiO_2 and TS.

Figure 10(a) shows the EPR spectra in the presence of TEMPO during the first 180 seconds of UV-Vis irradiation of TS suspensions. Similar results are obtained for TiO_2 (not shown). As already observed for the •DMPO-OH, the TEMPO signal decreases in intensity along the irradiation time (Figure 10(b)); as a consequence, the initial slope r_o of the TEMPO signal *versus* time was used as the representative parameter to evaluate the initial rate of $^1O_2$ formation.

Also in this case, the r_o value for pure TiO_2 is higher than the value for TS (Figure 8(b)), in accordance with the photocatalytic performances of the samples. The generation of TEMPO radicals in TiO_2 suspension increases up to

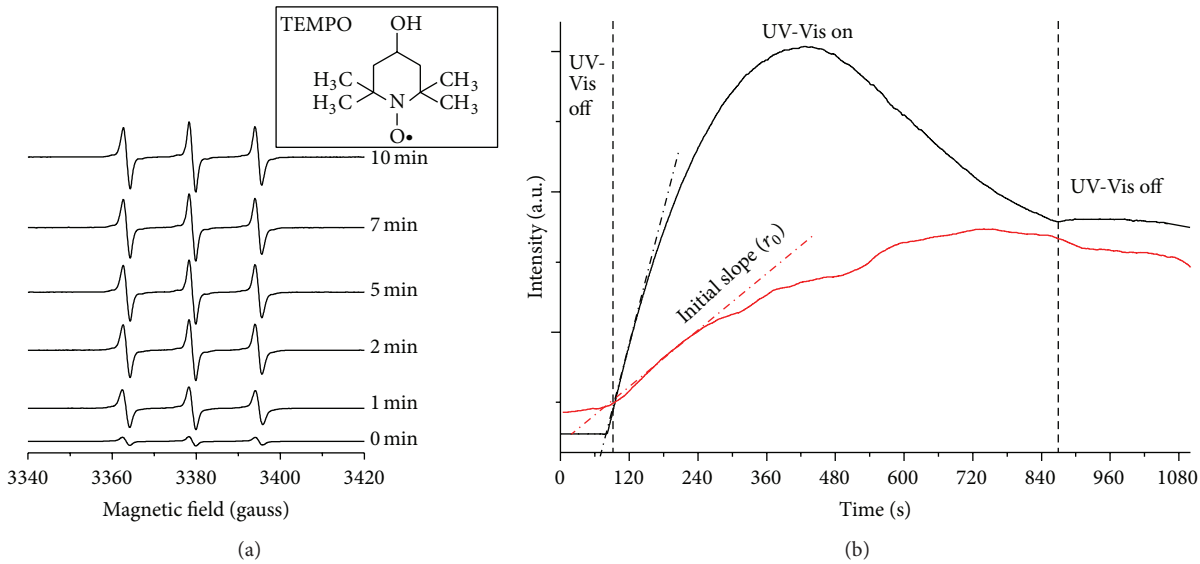

FIGURE 10: (a) Variation of resonance lines of the TEMPO radical (structure shown in the inset), with the UV-Vis irradiation time for the TS aqueous suspension; (b) time course of the TEMPO signal maximum before and during UV-Vis irradiation for TiO_2 (black line) and TS (red line) samples. The initial slope (r_o) of the curve was taken as representative parameter to evaluate the initial rate of $^1O_2$ formation.

~500 sec. and then rapidly decreases. Instead, in the presence of TS, the formation of radicals increases up to 700 sec. and then remains constant till the end of the irradiation time. This indicates, in analogy to the behavior of •DMPO-OH radicals, a higher stability of TEMPO radicals in TS composite than in TiO_2 and suggests that the coupling of TEMPO radicals is inhibited in TS due to the TiO_2 dispersion.

These results confirm a significant involvement of singlet oxygen in the photodegradation mechanism. In particular, the presence of $^1O_2$ species may be associated with the enhanced degradation of DCF and with the decomposition of its carbazole oxidation products. In fact, $^1O_2$ acts as an elective oxidant of electron-rich aromatic intermediate [43, 44], favoring their complete degradation.

In the present study, the formation rate and the concentration of different spin-trapped species have been used to measure the ROS yield and are connected to the catalytic behavior of the TiO_2 and TS samples. However, these data cannot be directly related to the degradation pathway of DCF because the spectra were acquired in the absence of the drug. Nevertheless, our investigation clearly demonstrates that a fair study of the titania-assisted photodegradation of pharmaceuticals must take into account the type, amount, and life time of different ROS species in order to understand the occurrence of specific catalytic performance.

4. Conclusions

The present study reports the oxidative photocatalytic degradation of 2-[2,6-(dichlorophenyl)amino]phenylacetic acid, DCF, in the presence of hydrothermal TiO_2 and TS materials as catalysts. The reaction was studied by UV-Vis absorption spectroscopy and by TOC determination.

It turned out that both TiO_2 and the TS composite display a remarkable efficiency in the degradation of the drug. Indeed DCF and its intermediate products, which resulted in being very stable under conventional and advanced water treatment, have been completely mineralized.

These results support the idea that the utilization of anatase nanocrystals with highly reactive exposed surfaces can be an effective tool for enhancing photooxidation reactions, even those of stable and persistent organic pollutants like DCF. Furthermore, the TiO_2 here employed, immobilized in silica matrix, preserves the functional properties of the unsupported active oxide, while allowing an easy technical use and recovery of the catalyst.

The catalysts performances have been related to the presence of three types of reactive oxygen species during the reaction, hydroxyl radicals (OH•), singlet oxygen ($^1O_2$), and superoxide ($O_2^{-\bullet}$). The formation of these ROS, assessed by EPR spin-trap experiments, indicates the significant involvement of singlet oxygen species in the DCF photodegradation.

It has also been suggested that ROS species do not easily quench in the titania-silica composite, thus increasing their possibility to be effective in the photodegradation process. This behavior may be ascribed to the high macro-/mesoporosity of the silica channels which tune the DMPO/•DMPO-OH diffusion toward/from the catalytic active sites, thus making gradual their interaction with the highly dispersed TiO_2 nanocrystals. This may prevent either the coupling or the fast photooxidation of •DMPO-OH radicals.

The nanocrystals act therefore as confined "nanoreactors," where ROS species form and can readily interact with the pollutants molecules.

To sum up, the substantially equal efficiencies of TiO_2 alone and TS, if referred to global mineralization times when

mineralization is completed, may be attributed, if not solely at least predominantly, to the stabilization effect of ROS by TS, in agreement with EPR results, which is able to change its kinetics in the early stage of photocatalytic mineralization process.

These innovative and unexpected properties of stabilization of oxygenated radicals exerted by the TS composite highlight the role of the reported immobilization procedure in preserving the functional properties of the photoactive oxide.

Conflict of Interests

The authors declare that there is no conflict of interests regarding the publication of this paper.

Acknowledgments

This work was in the frame of the European COST action MP1202 "Rational Design of Hybrid Organic Inorganic Interfaces: The Next Step towards Advanced Functional Materials." The authors thank Professor Stefano Polizzi of the University of Venezia for TEM analysis. M. Redaelli thanks Corimav for its support within the PCAM European Doctoral Programme.

References

[1] S. D. Richardson, "Water analysis: emerging contaminants and current issues," *Analytical Chemistry*, vol. 79, no. 12, pp. 4295–4324, 2007.

[2] K. Kümmerer, "Emerging Contaminants versus Micropollutants," *Clean—Soil, Air, Water*, vol. 39, no. 10, pp. 889–890, 2011.

[3] M. L. Farré, S. Pérez, L. Kantiani, and D. Barceló, "Fate and toxicity of emerging pollutants, their metabolites and transformation products in the aquatic environment," *TrAC—Trends in Analytical Chemistry*, vol. 27, no. 11, pp. 991–1007, 2008.

[4] K. Kümmerer, "Pharmaceuticals in the environment," *Annual Review of Environment and Resources*, vol. 35, no. 1, pp. 57–75, 2010.

[5] K. Fent, A. A. Weston, and D. Caminada, "Ecotoxicology of human pharmaceuticals," *Aquatic Toxicology*, vol. 76, no. 2, pp. 122–159, 2006.

[6] R. N. Brogden, R. C. Heel, G. E. Pakes, T. M. Speight, and G. S. Avery, "Diclofenac sodium: a review of its pharmacological properties and therapeutic use in rheumatic diseases and pain of varying origin," *Drugs*, vol. 20, no. 1, pp. 24–48, 1980.

[7] Y. Zhang, S.-U. Geißen, and C. Gal, "Carbamazepine and diclofenac: removal in wastewater treatment plants and occurrence in water bodies," *Chemosphere*, vol. 73, no. 8, pp. 1151–1161, 2008.

[8] T. A. Ternes and A. Joss, *Human Pharmaceuticals, Hormones and Fragrances. The Challenge of Micropollutants in Urban Water Management*, IWA Publishing, London, UK, 1st edition, 2007.

[9] E. C. Wert, F. L. Rosario-Ortiz, and S. A. Snyder, "Effect of ozone exposure on the oxidation of trace organic contaminants in wastewater," *Water Research*, vol. 43, no. 4, pp. 1005–1014, 2009.

[10] M. A. Abu-Hassan, J. K. Kim, I. S. Metcalfe, and D. Mantzavinos, "Kinetics of low frequency sonodegradation of linear alkylbenzene sulfonate solutions," *Chemosphere*, vol. 62, no. 5, pp. 749–755, 2006.

[11] J. Araña, J. A. H. Melián, J. M. D. Rodríguez et al., "TiO_2-photocatalysis as a tertiary treatment of naturally treated wastewater," *Catalysis Today*, vol. 76, no. 2–4, pp. 279–289, 2002.

[12] O. K. Dalrymple, D. H. Yeh, and M. A. Trotz, "Removing pharmaceuticals and endocrine-disrupting compounds from wastewater by photocatalysis," *Journal of Chemical Technology and Biotechnology*, vol. 82, no. 2, pp. 121–134, 2007.

[13] L. Prieto-Rodríguez, S. Miralles-Cuevas, I. Oller et al., "Optimization of mild solar TiO_2 photocatalysis as a tertiary treatment for municipal wastewater treatment plant effluents," *Applied Catalysis B: Environmental*, vol. 128, pp. 119–125, 2012.

[14] D. Kanakaraju, B. D. Glass, and M. Oelgemöller, "Titanium dioxide photocatalysis for pharmaceutical wastewater treatment," *Environmental Chemistry Letters*, vol. 12, no. 1, pp. 27–47, 2014.

[15] P. Calza, V. A. Sakkas, C. Medana et al., "Photocatalytic degradation study of diclofenac over aqueous TiO_2 suspensions," *Applied Catalysis B: Environmental*, vol. 67, no. 3-4, pp. 197–205, 2006.

[16] A. Achilleos, E. Hapeshi, N. P. Xekoukoulotakis, D. Mantzavinos, and D. Fatta-Kassinos, "Factors affecting diclofenac decomposition in water by UV-A/TiO_2 photocatalysis," *Chemical Engineering Journal*, vol. 161, no. 1-2, pp. 53–59, 2010.

[17] M. Schmitt-Jansen, P. Bartels, N. Adler, and R. Altenburger, "Phytotoxicity assessment of diclofenac and its phototransformation products," *Analytical and Bioanalytical Chemistry*, vol. 387, no. 4, pp. 1389–1396, 2007.

[18] R. Scotti, M. D'Arienzo, A. Testino, and F. Morazzoni, "Photocatalytic mineralization of phenol catalyzed by pure and mixed phase hydrothermal titanium dioxide," *Applied Catalysis B: Environmental*, vol. 88, no. 3-4, pp. 497–504, 2009.

[19] R. Nakamura and Y. Nakato, "Primary intermediates of oxygen photoevolution reaction on TiO_2 (Rutile) particles, revealed by in situ FTIR absorption and photoluminescence measurements," *Journal of the American Chemical Society*, vol. 126, no. 4, pp. 1290–1298, 2004.

[20] Y. Nosaka and H. Fukuyama, "Application of chemiluminescent probe to the characterization of TiO_2 photocatalysts in aqueous suspension," *Chemistry Letters*, no. 4, pp. 383–384, 1997.

[21] Y. Nosaka, Y. Yamashita, and H. Fukuyama, "Application of chemiluminescent probe to monitoring superoxide radicals and hydrogen peroxide in TiO_2 photocatalysis," *Journal of Physical Chemistry B*, vol. 101, no. 30, pp. 5822–5827, 1997.

[22] K. Ishibashi, Y. Nosaka, K. Hashimoto, and A. Fujishima, "Time-dependent behavior of active oxygen species formed on photoirradiated TiO_2 films in air," *The Journal of Physical Chemistry B*, vol. 102, no. 12, pp. 2117–2120, 1998.

[23] R. Konaka, E. Kasahara, W. C. Dunlap, Y. Yamamoto, K. C. Chien, and M. Inoue, "Irradiation of titanium dioxide generates both singlet oxygen and superoxide anion," *Free Radical Biology and Medicine*, vol. 27, no. 3-4, pp. 294–300, 1999.

[24] T. Hirakawa, K. Yawata, and Y. Nosaka, "hotocatalytic reactivity for $O_{2\cdot}^-$ and OH· radical formation in anatase and rutile TiO_2 suspension as the effect of H_2O_2 addition," *Applied Catalysis A: General*, vol. 325, pp. 105–111, 2007.

[25] S.-K. Han, R. H. Sik, A. G. Motten, C. F. Chignell, and P. J. Bilski, "Photosensitized oxidation of tetrabromobisphenol a by humic

acid in aqueous solution," *Photochemistry and Photobiology*, vol. 85, no. 6, pp. 1299–1305, 2009.

[26] B. Razavi, S. B. Abdelmelek, W. Song, K. E. O'Shea, and W. J. Cooper, "Photochemical fate of atorvastatin (lipitor) in simulated natural waters," *Water Research*, vol. 45, no. 2, pp. 625–631, 2011.

[27] O. C. Romero, A. P. Straub, T. Kohn, and T. H. Nguyen, "Role of temperature and suwannee river natural organic matter on inactivation kinetics of rotavirus and bacteriophage MS2 by solar irradiation," *Environmental Science and Technology*, vol. 45, no. 24, pp. 10385–10393, 2011.

[28] D. Gryglik, J. S. Miller, and S. Ledakowicz, "Singlet molecular oxygen application for 2-chlorophenol removal," *Journal of Hazardous Materials*, vol. 146, no. 3, pp. 502–507, 2007.

[29] C. S. Foote and J. W. Peters, "Chemistry of singlet oxygen. XIV. Reactive intermediate in sulfide photooxidation," *Journal of the American Chemical Society*, vol. 93, pp. 3795–3796, 1971.

[30] M. C. De Rosa and R. J. Crutchley, "Photosensitized singlet oxygen and its applications," *Coordination Chemistry Reviews*, vol. 234, pp. 351–371, 2002.

[31] M. D'Arienzo, M. Crippa, A. A. Essawy et al., "Membrane-assisted charge separation and photocatalytic activity in embedded TiO_2: a kinetic and mechanistic study," *Journal of Physical Chemistry C*, vol. 114, no. 37, pp. 15755–15762, 2010.

[32] L. Reijnders, "Hazard reduction for the application of titania nanoparticles in environmental technology," *Journal of Hazardous Materials*, vol. 152, no. 1, pp. 440–445, 2008.

[33] W.-J. Ong, L.-L. Tan, S.-P. Chai, S.-T. Yong, and A. R. Mohamed, "Facet-dependent photocatalytic properties of TiO_2-based composites for energy conversion and environmental remediation," *ChemSusChem*, vol. 7, no. 3, pp. 690–719, 2014.

[34] J. Pan, G. Liu, G. Qing, M. Lu, and H.-M. Cheng, "On the true photoreactivity order of 001, 010, and 101 facets of anatase TiO_2 crystals," *Angewandte Chemie International Edition*, vol. 50, pp. 2133–2137, 2011.

[35] A. G. Thomas, W. R. Flavell, A. K. Mallick et al., "Comparison of the electronic structure of anatase and rutile TiO_2 single-crystal surfaces using resonant photoemission and x-ray absorption spectroscopy," *Physical Review B*, vol. 75, no. 3, Article ID 035105, 12 pages, 2007.

[36] A. Testino, I. R. Bellobono, V. Buscaglia et al., "Optimizing the photocatalytic properties of hydrothermal TiO_2 by the control of phase composition and particle morphology. A systematic approach," *Journal of the American Chemical Society*, vol. 129, no. 12, pp. 3564–3575, 2007.

[37] M. Crippa, E. Callone, M. D'Arienzo et al., "TiO_2 nanocrystals grafted on macroporous silica: a novel hybrid organic-inorganic sol-gel approach for the synthesis of highly photoactive composite material," *Applied Catalysis B: Environmental*, vol. 104, no. 3-4, pp. 282–290, 2011.

[38] F. Morazzoni, R. Scotti, M. Crippa, and M. D'Arienzo, United States Patent Application Publication US 20130153483 A1 20130620, 2013.

[39] M. Lazzeri, A. Vittadini, and A. Selloni, "Structure and energetics of stoichiometric TiO_2 anatase surfaces," *Physical Review B*, vol. 63, Article ID 155409, pp. 1–8, 2001.

[40] L. Ye, J. Mao, T. Peng, L. Zan, and Y. Zhang, "Opposite photocatalytic activity orders of low-index facets of anatase TiO_2 for liquid phase dye degradation and gaseous phase CO_2 photoreduction," *Physical Chemistry Chemical Physics*, vol. 16, pp. 15675–15680, 2014.

[41] M. D'Arienzo, J. Carbajo, A. Bahamonde et al., "Photogenerated defects in shape-controlled TiO_2 anatase nanocrystals: a probe to evaluate the role of crystal facets in photocatalytic processes," *Journal of the American Chemical Society*, vol. 133, no. 44, pp. 17652–17661, 2011.

[42] Z. Zheng, B. Huang, J. Lu, X. Qin, X. Zhang, and Y. Dai, "Hierarchical TiO_2 microspheres: synergetic effect of 001 and 101 facets for enhanced photocatalytic activity," *Chemistry*, vol. 17, no. 52, pp. 15032–15038, 2011.

[43] J. Eriksson, J. Svanfelt, and L. Kronberg, "A photochemical study of diclofenac and its major transformation products," *Photochemistry and Photobiology*, vol. 86, no. 3, pp. 528–532, 2010.

[44] J. Svanfelt, J.-M. Kallio, J. Eriksson, and L. Kronberg, "Environmental fate and hazards of the pharmaceutical diclofenac in aquatic environments," in *Contaminants of Emerging Concern in the Environment: Ecological and Human Health Considerations*, R. U. Halder, Ed., ACS Symposium Series, chapter 11, pp. 243–255, American Chemical Society, Washington, DC, USA, 2010.

[45] F. Rota, M. Cavassi, D. Niego et al., "Mathematical modelling of photomineralization of phenols in aqueous solution, by photocatalytic membranes immobilizing titanium dioxide," *Chemosphere*, vol. 33, no. 11, pp. 2159–2173, 1996.

[46] I. R. Bellobono, F. Morazzoni, R. Bianchi et al., "Laboratory-scale photomineralisation of n-alkanes in aqueous solution, by photocatalytic membranes immobilising titanium dioxide," *International Journal of Photoenergy*, vol. 7, no. 2, pp. 79–85, 2005.

[47] I. R. Bellobono, R. Bianchi, G. De Martini et al., "Nonlinear modelling of data in photomineralization kinetics of organic micropollutants by photocatalytic membranes immobilizing titanium dioxide in membrane reactors," *Journal of Chemometrics*, vol. 22, no. 7, pp. 425–435, 2008.

[48] A. Fujishima, T. N. Rao, and D. A. Tryk, "Titanium dioxide photocatalysis," *Journal of Photochemistry and Photobiology C: Photochemistry Reviews*, vol. 1, no. 1, pp. 1–21, 2000.

[49] D. T. Sawyer and J. S. Valentine, "How super is superoxide?" *Accounts of Chemical Research*, vol. 14, no. 12, pp. 393–400, 1981.

[50] E. G. Janzen, C. C. Lai, and R. V. Shetty, "Electron spin resonance spectrum of a 5-membered cyclic alkoxy nitroxyl radical," *Tetrahedron Letters*, vol. 21, no. 13, pp. 1201–1204, 1980.

[51] P. Bilski, K. Reszka, M. Bilska, and C. F. Chignell, "Oxidation of the spin trap 5,5-dimethyl-1-pyrroline *N*-oxide by singlet oxygen in aqueous solution," *Journal of the American Chemical Society*, vol. 118, no. 6, pp. 1330–1338, 1996.

[52] G. M. Liu, X. Z. Li, J. C. Zhao, S. Horikoshi, and H. Hidaka, "Photooxidation mechanism of dye alizarin red in TiO_2 dispersions under visible illumination: an experimental and theoretical examination," *Journal of Molecular Catalysis A: Chemical*, vol. 153, pp. 221–229, 2000.

[53] S. K. Han, T.-M. Hwang, Y. Yoon, and J.-W. Kang, "Evidence of singlet oxygen and hydroxyl radical formation in aqueous goethite suspension using spin-trapping electron paramagnetic resonance (EPR)," *Chemosphere*, vol. 84, no. 8, pp. 1095–1101, 2011.

[54] R. Konaka, E. Kasahara, W. C. Dunlap, Y. Yamamoto, K. C. Chien, and M. Inoue, "Ultraviolet irradiation of titanium dioxide in aqueous dispersion generates singlet oxygen," *Redox Report*, vol. 6, no. 5, pp. 319–325, 2001.

[55] V. Brezová, D. Dvoranová, and A. Staško, "Characterization of titanium dioxide photoactivity following the formation of radicals by EPR spectroscopy," *Research on Chemical Intermediates*, vol. 33, no. 3–5, pp. 251–268, 2007.

[56] A. Kubacka, G. Colon, and M. Fernandez-Garcia, "N- and/or W-(co)doped TiO_2-anatase catalysts: effect of the calcination treatment on photoactivity," *Applied Catalysis B: Environmental*, vol. 95, pp. 238–244, 2010.

[57] T. Daimon, T. Hirakawa, M. Kitazawa, J. Suetake, and Y. Nosaka, "Formation of singlet molecular oxygen associated with the formation of superoxide radicals in aqueous suspensions of TiO_2 photocatalysts," *Applied Catalysis A: General*, vol. 340, no. 2, pp. 169–175, 2008.

[58] P. Wang, Y. Tang, Z. Dong, Z. Chen, and T.-T. Lim, "Ag-AgBr/TiO_2/RGO nanocomposite for visible-light photocatalytic degradation of penicillin G," *Journal of Materials Chemistry A*, vol. 1, no. 15, pp. 4718–4727, 2013.

[59] O. Moan and E. Wold, "Detection of singlet oxygen production by ESR," *Nature*, vol. 179, pp. 450–451, 1979.